Steel and Composite Structures, *Vol. 34, No. 1* (*2020*) *17-34*
DOI: https://doi.org/10.12989/scs.2020.34.1.017

Flexural behavior of beams reinforced with either steel bars, molded or pultruded GFRP grating

Muhammad N.S. Hadi*, Mohammed H.A. Almalome, Tao Yu and William A. Rickards

School of Civil, Mining and Environmental Engineering, University of Wollongong, Wollongong, NSW 2522, Australia

(*Received July 29, 2019, Revised October 16, 2019, Accepted October 21, 2019*)

Abstract. This paper investigates the flexural behavior of concrete beams reinforced longitudinally with either steel bars, molded glass-fiber reinforced polymer (GFRP) grating mesh or pultruded glass-fiber reinforced polymer (GFRP) grating mesh, under four-point bending. The variables included in this study were the type of concrete (normal weight concrete, perlite concrete and vermiculite concrete), type of the longitudinal reinforcement (steel bars, molded and pultruded GFRP grating mesh) and the longitudinal reinforcement ratio (between 0.007 and 0.035). The influences of these variables on the load-midspan deflection curves, bending stiffness, energy absorption and failure modes were investigated. A total of fifteen beams with a cross-sectional dimension of 160 mm × 210 mm and an overall length of 2400 mm were cast and divided into three groups. The first group was constructed with normal weight concrete and served as a reference concrete. The second and third groups were constructed with perlite concrete and vermiculite concrete, respectively. An innovative type of stirrup was used as shear reinforcement for all beams. The results showed that the ultimate load of the beams reinforced with pultruded GFRP grating mesh ranged between 19% and 38% higher than the ultimate load of the beams reinforced with steel bars. The bending stiffness of all beams was influenced by the longitudinal reinforcement ratio rather than the type of concrete. Failure occurred within the pure bending region which means that the innovative stirrups showed a significant resistance to shear failure. Good agreement between the experimental and the analytical ultimate load was obtained.

Keywords: molded GFRP grating; pultruded GFRP grating; expanded perlite; expanded vermiculite; energy absorption

1. Introduction

Different types of steel reinforcement such as steel bars and steel plates are commonly used in combination with concrete as longitudinal reinforcement or strengthening materials, due to the well-established knowledge of their behavior and their desirable properties (Chen and Wang 2015, Xiao *et al.* 2017, Xiong *et al.* 2012). However, steel materials have an issue of being susceptible to chloride-induced corrosion, especially when used for structures built in corrosive environments (Alsayed 1998). Therefore, fiber reinforced polymer (FRP) composites have been used as a replacement for the conventional steel bars in reinforced concrete structures, because of its high corrosion resistance, excellent durability and lightweight nature (Barris *et al.* 2009, Kalpana and Subramanian 2011, El-Nemr *et al.* 2013, Goldston *et al.* 2016).

Over the years, there have been research studies about the flexural behavior of GFRP composite reinforced concrete beams under four-point bending. Alsayed (1998) and Goldston *et al.* (2016) reported that increasing the longitudinal reinforcement ratio of concrete beams resulted in an improvement in the bending stiffness after first crack load. Barris *et al.* (2009) reported that the beams with low longitudinal reinforcement ratio experienced a large midspan deflection and the dominant failure was caused by GFRP rupture. Kalpana and Subramanian (2011) confirmed that increasing the longitudinal reinforcement ratio of the concrete beams reinforced with GFRP bars resulted in an increase in the ultimate load. El-Nemr *et al.* (2013) confirmed that beams designed to fail by concrete crushing experienced higher ductility than the beams that failed due to GFRP rupture.

Molded GFRP grating mesh and pultruded GFRP grating mesh are composite materials of a polymer matrix reinforced with glass-fiber. The percentage of glass-fiber in the molded and pultruded GFRP grating mesh ranged between 32% and 41% and the percentage of resin ranged between 59% and 68% (American grating 2015). Molded and pultruded GFRP gratings have only been used as longitudinal reinforcement in one-way concrete slabs by a limited number of researchers (Larralde 1992, Biddah 2006). Larralde (1992) confirmed that the shear span length-to-effective depth ratio of less than five for slabs reinforced with molded GFRP grating mesh produced a GFRP rupture failure. Biddah (2006) confirmed that using a longitudinal reinforcement ratio for the slabs reinforced with pultruded GFRP grating mesh of 75% higher than the slabs reinforced with steel bars led to an increase in the ultimate load to about 15% higher than the slabs reinforced with steel bars

The demand in industry for a new lightweight construction material with low bulk density has led to the

*Corresponding author, Associate Professor
E-mail: mhadi@uow.edu.au

http://www.techno-press.org/?journal=scs&subpage=6
ISSN: 1229-9367 (Print), 1598-6233 (Online)

Table 1 Mix proportions of perlite concrete and vermiculite concrete

Materials	Perlite concrete	Vermiculite concrete
Cement kg/m^3	755	770
Fine aggregate kg/m^3	400	590
Coarse aggregate kg/m^3	500	530
Expanded perlite kg/m^3	70	-
Expanded vermiculite kg/m^3	-	40
Pre-absorption water kg/m^3	140	80
Water l/m^3	185	267
WRA* l/m^3	3.4	3.5

* WRA: Water reducing admixture (Plastiment® -10) (Sika 2017)

research about lightweight concrete. Accordingly, materials such as expanded perlite and expanded vermiculite have been used to produce lightweight concrete (Rashad 2016a). Expanded perlite is an amorphous volcanic silicate rock with low thermal conductivity and low bulk density (Rashad 2016a). Similarly, expanded vermiculite is a hydrous phyllosilicate mineral which also has low thermal conductivity and low bulk density (Rashad 2016b). Schackow *et al.* (2014), Demirboga *et al.* (2001), Abdeen and Hodhod (2010) and Oktay *et al.* (2015) have either partially or totally replaced the fine aggregate and coarse aggregate with the expanded perlite and expanded vermiculite in the concrete mixtures (the replacement ranged between 20% and 100% by volume). They were found that a bulk density ranged from 750 kg/m^3 to 1900 kg/m^3 and a corresponding 28 day compressive strength between 12 MPa and 19 MPa were obtained.

To summarize, the use of molded GFRP grating mesh and pultruded GFRP grating mesh as longitudinal reinforcement in concrete beams has not yet been the focus of research. Similarly, using the expanded perlite and expanded vermiculite in concrete have led to a reduction in the overall weight of concrete. However, achieving adequate compressive strength for structural purposes is still an issue that remains to be resolved.

In this study, either steel bars, molded GFRP grating mesh or pultruded GFRP grating mesh have been used as longitudinal reinforcement in concrete beams. Three types of concrete were used in this study including normal weight concrete, concrete containing expanded perlite and concrete containing expanded vermiculite. The normal weight concrete used in this study referred as reference concrete. The concrete containing expanded perlite used in this study served as perlite concrete. The concrete containing expanded vermiculite used in this study served as vermiculite concrete. The perlite concrete and vermiculite concrete were obtained from a total of eighteen concrete trial mixes. The aim of this study is to investigate the influences of the type of concrete (the reference concrete, perlite concrete and vermiculite concrete), the type of longitudinal reinforcement (steel bars, molded GFRP grating mesh and pultruded GFRP grating mesh) and the longitudinal reinforcement ratio (between 0.007 and 0.035) on the load-midspan deflection curves, bending stiffness, energy absorption and failure modes of beams tested under four-point bending. For all beams, an innovative type of stirrup (sand coated carbon-fiber reinforced polymer; SCCFRP) was constructed and used as shear reinforcement instead of steel bars.

2. Experimental program

2.1 Material properties

Material properties were divided into three parts, namely, properties of concrete, properties of the longitudinal reinforcement and properties of an innovative shear reinforcement (sand coated carbon-fiber reinforced polymer, SCCFRP).

2.1.1 Properties of concrete

Three types of concrete were produced in this study, namely, normal weight concrete (reference concrete), perlite concrete and vermiculite concrete. The reference concrete was supplied by Hanson Construction and Building Materials (2017). The perlite concrete and vermiculite concrete batches were obtained from a total of eighteen concrete trial mixes. The mix proportions of perlite concrete and vermiculite concrete are reported in Table 1. The perlite concrete and vermiculite concrete mixes consist of the following materials: general purpose cement, fine aggregate with a maximum size of 4 mm, coarse aggregate with a maximum size of 10 mm, expanded perlite with a maximum size of 5 mm, expanded vermiculite with a maximum size of 5 mm, water and water reducing admixture (Plastiment® -10) (Sika 2012). The expanded perlite and expanded vermiculite were supplied by Ausperl (2012). Perlite concrete and vermiculite concrete were cast, cured and tested in the civil engineering laboratories, University of Wollongong, Australia.

Before mixing the ingredients used to produce the perlite concrete and vermiculite concrete, it was important to measure the amount of water that could be absorbed (water absorption) by expanded perlite and expanded vermiculite. The purpose of measuring the water absorption was to ensure that the effective water/cement ratio did not get affected by the tendency of the expanded perlite and expanded vermiculite to absorb water during the concrete mixing process. The water absorption of expanded perlite and expanded vermiculite was measured based on AS 2758.1 (2009). Water absorption of 200% by weight for each of expanded perlite and expanded vermiculite was obtained. Based on this measurement, a certain quantity of pre-absorption water was specified for each mix (perlite concrete and vermiculite concrete), equal to double the weight of either the expanded perlite or expanded vermiculite in the concrete mix (Table 1). For each of perlite concrete and vermiculite concrete mixing, the quantity of pre-absorption water was added to the expanded perlite and expanded vermiculite for approximately 30 min before adding the remaining ingredients (cement, fine aggregate, coarse aggregate and water), inside a drum mixer. Then, the cement, fine aggregate and coarse aggregate were added inside a drum mixer and mixed with either expanded perlite or expanded vermiculite. The water and the water reducing admixture (Plastiment®-10) were then pre-mixed and added gradually to the concrete mix. The total mixing time of perlite concrete and vermiculite concrete was approximately 5 to 6 min.

A total of 18 concrete cylinders with a 100 mm diameter and a 200 mm height were cast and tested under compression. The 18 concrete cylinders included six cylinders for the reference concrete, six cylinders for the perlite concrete and six cylinders of the vermiculite concrete. The six cylinders for each type of concrete included three cylinders tested at 28 days and the remaining three cylinders tested at the age of testing the beams. In addition, a total of nine concrete cylinders with a 150 mm diameter and 300 mm height were cast and tested under compression. The nine cylinders included three cylinders for each type of concrete. The cylinders with a 150 mm diameter and 300 height have been used to determine the average compressive modulus of elasticity at the age of testing the beams. The average compressive modulus of elasticity was calculated using the chord method based on AS 1012 (1999). Table 2 reports the compressive strength and the compressive modulus of elasticity of the concrete. At 28 days, the average compressive strengths of the reference concrete, perlite concrete and vermiculite concrete were 40 MPa, 36 MPa and 28 MPa, respectively. At the age of testing beams, the average compressive strengths of the reference concrete, perlite concrete and vermiculite concrete were 44 MPa, 40 MPa and 32 MPa, respectively (Table 2). At the age of testing beams, the average compressive modulus of elasticity of the reference concrete, perlite concrete and vermiculite concrete were 28.5 GPa, 20.3 GPa and 17.0 GPa, respectively (Table 2).

2.1.2 Properties of the longitudinal reinforcement

The tensile properties of the 12 mm diameter deformed steel bars (N12) and 6 mm diameter plain rounded steel bars (R6) were obtained by tensile testing based on AS 1391 (2007). The average tensile yield stress of three bars for N12 was 586 MPa (Table 3). The average tensile yield stress of three bars for R6 was 556 MPa respectively (Table 3).

The molded GFRP grating mesh and pultruded GFRP grating mesh were supplied by Scavenger (2015). The ratio of the weight of the glass-fiber to the total weight of these GFRP composites (molded and pultruded GFRP gratings) ranged from 32% to 41% (American grating 2015). To determine the tensile properties of these reinforcements, three segments for each type of GFRP gratings with a length of 750 mm were cut from the mesh and tested under tensile loading. For this tensile test, a new approach has been developed by fabricating a steel anchor (Fig. 1(a)). The steel anchor was constructed with two steel angles. Each steel angle was 20 mm thick, with 70 mm length of one leg and 130 mm length of the other leg. The cross-sectional dimensions of the steel angle are shown in Fig. 1(b). The two steel angles were connected using 8M10 × 30 mm bolts to form a box with a rectangular cross-sectional steel anchor. These bolts included 4M10 × 30 bolts located on each side of the anchor. The spacing between the M10 × 30 bolts was 80 mm center to center. The cross-sectional dimensions of the anchor (Section A-A) are shown in Fig. 1(c). The inside cross-sectional dimensions of the steel anchor were 50 mm × 90 mm, as shown in Fig. 1(c).

Fig. 2(a) shows the anchor and the universal joint connected by using a steel plate to form a single part. One steel plate with the dimensions of 20 mm × 90 mm × 130 mm was welded at the end of one of the steel angles and connected with the other by a 1M10 × 30 mm bolt located in the corner. The main purpose of using this steel plate was to connect the universal joint to the steel anchors to form a single part. Three steel pins with the dimensions of 5 mm × 5 mm × 20 mm were welded inside each steel angle. Fig. 2(b) shows more details of the three welded pins and the welded plate located at one steel angle. The center-to-center spacing between the welded pins was 85 mm (Fig. 2(b)). Expansive cement was used to fix the ends of a GFRP segment (GFRP grating) to the anchors (the length of the end of each segment was 300 mm). A universal joint was used to connect the anchors (rectangular steel formwork) to the testing machine. The length of the universal joint was 360 mm. This included an 80 mm circular steel rod used for the testing machine to grip during the testing (Fig. 1(a)). The universal joint was designed by Alhussainy *et al.* (2017). Three segments for each type of GFRP grating were tested under tension with a displacement rate of 1 mm/min.

Referring to Table 3, the average tensile strength and the average tensile modulus of elasticity of 25 mm overall depth molded GFRP grating (MG-25) were 190 MPa and 15 GPa, respectively. The average tensile strength and the average tensile modulus of elasticity of 38 mm overall depth molded GFRP grating (MG-38) were 275 MPa and 16 GPa, respectively. The average tensile strength and the average tensile modulus of elasticity of 38 mm overall depth I-section pultruded GFRP grating (PGI-38) were 315 MPa and 24 GPa, respectively. Finally, the average tensile strength and the average tensile modulus of elasticity of 38 mm overall depth T-section pultruded GFRP grating (PGT-38) were 361 MPa and 28 GPa, respectively.

The GFRP bars with a diameter of 6.35 (#2) were supplied by V-rod (2012). The tensile properties of the 6.35 mm diameter GFRP bars (#2) were obtained by tensile testing based on ASTM D7205 (2011). For this tensile test, two cylindrical steel anchors with 16 mm inner diameter

Table 2 Mechanical properties of concrete

Type of concrete	Average bulk density (kg/m^3)	Average compressive strength at 28 days (MPa)	Average compressive strength at the age of testing beams (MPa)	Average modulus of elasticity (GPa)
Reference concrete	2413	40	44	28.5
Perlite concrete	1910	36	40	20.3
Vermiculite concrete	2120	28	32	17.0

Table 3 Properties of the reinforcement

Material	Average tensile yield stress (MPa)	Average tensile yield strain (%)	Average tensile strength (MPa)	Average tensile rupture strain (%)	Modulus of elasticity (GPa)
N12	586	0.31	-	-	190
R6	556	0.27	-	-	211
#2	-	-	975	1.8	54
MG-25	-	-	190	1.2	15
MG-38	-	-	275	1.7	16
PGI-38	-	-	315	1.3	24
PGT-38	-	-	361	1.3	28
CFRP sheet	-	-	519	1.3	43

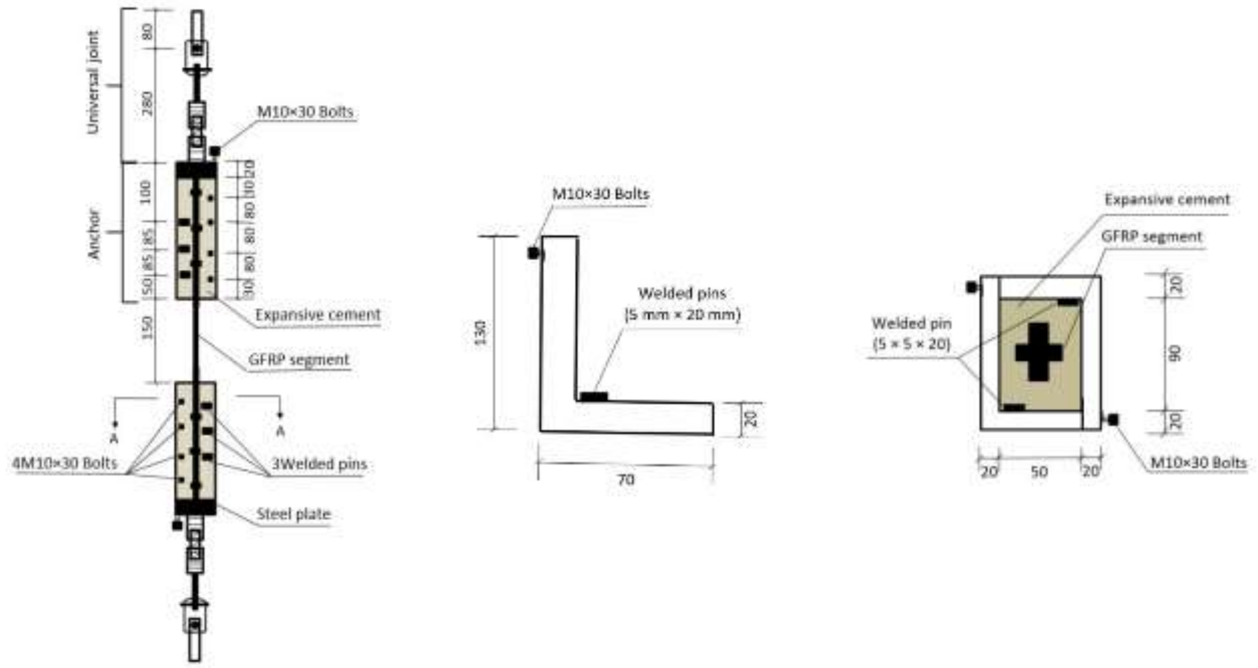

(a) Side view of anchors and universal joints

(b) Cross-section of L-shape steel angle

(c) Cross-sectional dimensions of the anchor

Fig. 1 Tensile test method of a GFRP segment (all dimensions in mm)

and 26 mm outer diameter were filled with expansive cement to fix the ends of the GFRP bars. The length of each of these steel anchors was 300 mm (Fig. 3). Four PVC caps with central holes fitting the GFRP bar were placed at the top and bottom ends of each anchor (Fig. 3). The PVC caps were used to ensure that the ends of the GFRP bar were located in the center of the inner diameter of the cylindrical steel anchor, providing a clear mortar cover of 4.8 mm (Fig. 3). During the test, a plastic shield was placed in front of the testing machine to prevent fibers from flying across the room in the event of rupture of a GFRP bar. The average test results of three GFRP bars are shown in Table 3. The

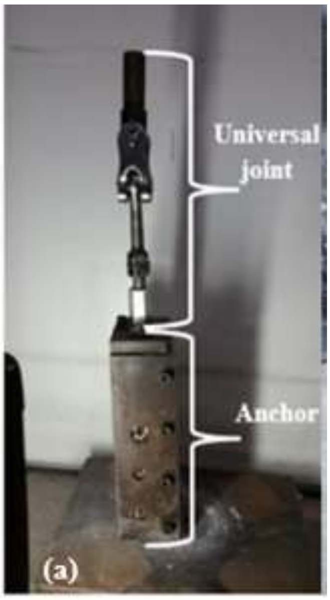

(a) The anchor and the universal joint connected by using a steel plate

(b) The details of the three pins inside the anchor

Fig. 2 The anchor and the universal joint

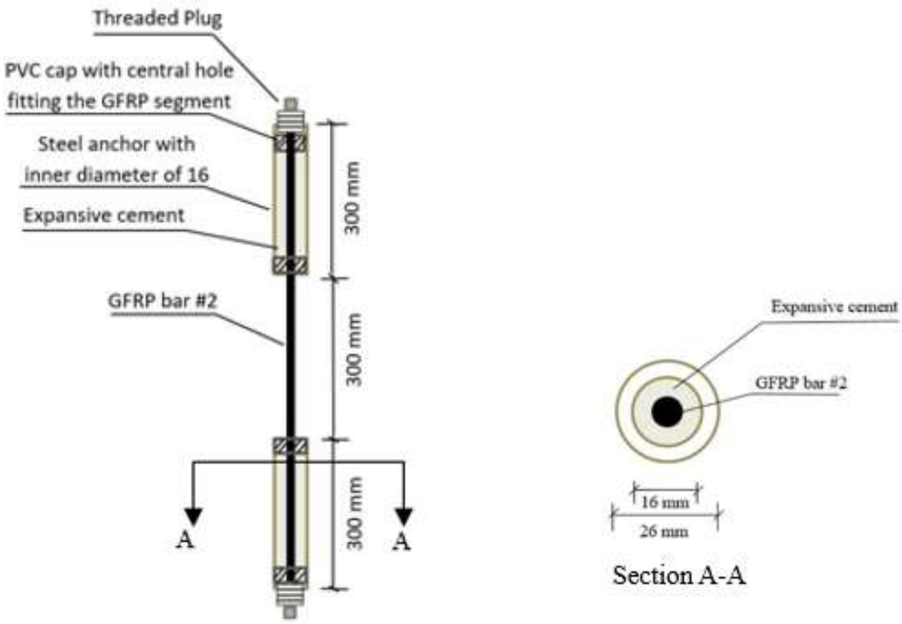

Fig. 3 Details of the tensile test of 6.35 mm diameter GFRP bar (#2)

average tensile strength and the average tensile modulus of elasticity of 6.35 mm (#2) diameter GFRP bars were 975 MPa and 54 GPa, respectively.

2.1.3 Properties of an innovative stirrup

An innovative type of stirrup known as sand coated carbon- fiber reinforced polymer (SCCFRP) was constructed and used as shear reinforcement for all beams. The materials used to produce these innovative stirrups were: sheets of carbon-fiber, a thermosetting resin (epoxy) and fine aggregate (sand) with a maximum size of 4 mm. Fig. 4 shows the SCCFRP stirrup being manufactured. The first step of manufacturing the stirrups was to prepare a rectangular plywood, which was then used as a formwork to manufacture the SCCFRP stirrups (Fig. 4). The outer cross-sectional dimensions of this formwork were 120 mm × 170 mm with an overall length of 1200 mm. In the second step, a plastic sheet was wrapped around this plywood formwork

Fig. 4 The process of manufacturing the SCCFRP stirrups

to avoid the SCCFRP sheet sticking to the plywood during the construction of the stirrups (Fig. 4). In the third step, a sheet of carbon-fiber with a 100 mm width and 1200 mm length was saturated with a thermosetting resin on both faces. In the fourth step, the fine aggregate (sand) was smeared over the entire length of the CFRP sheet. Then, the sheet of carbon-fiber was folded along its longitudinal axis. This led to the formation of two layers of SCCFRP sheet, with width reduced from 100 mm to 50 mm. In the last step, the folded SCCFRP sheet was wrapped twice around the plywood formwork (Fig. 4). This resulted in four layers of SCCFRP sheet with an overall thickness of 5 mm and a width of 50 mm for each stirrup. The constructed stirrups were left to cure for two days, before being used in the beams.

Five coupons of CFRP sheet with the measured dimensions of 1 mm × 25 mm × 250 mm were tested under tensile loading based on ASTM D3039 (2000) to determine their tensile properties. The average tensile strength and average tensile modulus of elasticity of the CFRP sheets were 519 MPa and 43 GPa, respectively (Table 3).

2.2 Details of beams

A total of fifteen beams with a cross-sectional dimension of 160 mm × 210 mm and an overall beam length of 2400 mm were cast and tested under four-point bending. The fifteen beams were divided into three groups based on the type of concrete. The three groups included the reference concrete (R) as a first group, perlite concrete (P) as a second group and vermiculite concrete (V) as a third group. Each group consisted of five beams. Figs. 5(a)-5(e) show the details of the cross-sectional dimensions of the five beams at each group. Referring to Figs. 5 (a)-5(e), the beams were labeled in three parts. The first part represents the type of concrete (the reference concrete, R; perlite concrete, P; and vermiculite concrete, V). The second part refers to the type of the longitudinal reinforcement in tension (steel bars, S; molded GFRP grating mesh, MG; pultruded I-cross sectional shape GFRP grating mesh, PGI; and pultruded T-cross sectional shape GFRP grating mesh, PGT). The third part represents the diameter of the steel bars (12 mm) or the overall depth of molded and pultruded GFRP grating mesh (25 mm or 38 mm). For example, Beam R-PGT-38 represents the concrete beam constructed with the reference concrete (R), reinforced with pultruded GFRP grating mesh of T-cross sectional shape (PGT) and 38 mm overall reinforcement depth. Table 4 reports the number and location of the top reinforcement (Compression) and bottom reinforcement (Tension) in the beam cross sections.

Referring to Fig. 5 and Table 4, the five beams at each group were reinforced with five types of reinforcement in tension (bottom reinforcement). The first beam was reinforced in tension with two deformed steel bars of 12 mm diameter (Fig. 5(a)). The second beam was reinforced in tension with four bars of 25 mm overall depth molded GFRP grating mesh (Fig. 5(b)). The third beam was reinforced in tension with four bars of 38 mm overall depth molded GFRP grating mesh (Fig. 5(c)). The fourth beam was reinforced in tension with four bars of 38 mm overall depth I-cross sectional shape pultruded GFRP grating mesh (Fig. 5(d)). The fifth beam was reinforced in tension with three bars of 38 mm overall depth T-cross sectional shape pultruded GFRP grating mesh (Fig. 5(e)). In addition, two types of compression reinforcement have been used to reinforce the five beams at each group. Only the first beam at each group (R-S-12, P-S-12 and V-S-12) was reinforced in compression with two plain rounded steel bars of 6 mm diameter (Fig. 5(a)) while the remaining four beams at each group were reinforced in compression with two GFRP bars of 6.35 mm diameter, (Figs. 5 (b)-5(e)). All the beams in all

Table 4 number and location the reinforcement in beam cross-sections

Group	Beam	Beam cross-sectional dimensions (mm)	Top reinforcement	Bottom reinforcement
	R-S-12	160 × 210	2R6	2N12
	R-MG-25	160 × 210	2#2 GFRP	4MG-25
R*	R-MG-38	160 × 210	2#2 GFRP	4MG-38
	R-PGI-38	160 × 210	2#2 GFRP	4PGI-38
	R-PGT-38	160 × 210	2#2 GFRP	3PGT-38
	P-S-12	160 × 210	2R6	2N12
	P-MG-25	160 × 210	2#2 GFRP	4MG-25
P*	P-MG-38	160 × 210	2#2 GFRP	4MG-38
	P-PGI-38	160 × 210	2#2 GFRP	4PGI-38
	P-PGT-38	160 × 210	2#2 GFRP	3PGT-38
	V-S-12	160 × 210	2R6	2N12
	V-MG-25	160 × 210	2#2 GFRP	4MG-25
V*	V-MG-38	160 × 210	2#2 GFRP	4MG-38
	V-PGI-38	160 × 210	2#2 GFRP	4PGI-38
	V-PGT-38	160 × 210	2#2 GFRP	3PGT-38

* R: Reference concrete; P: Perlite concrete; V: Vermiculite concrete

the three groups were reinforced for shear with stirrups of the sand coated carbon-fiber reinforced polymer (SCCFRP) (Fig. 5).

Table 5 reports more details regarding the effective depth and longitudinal reinforcement ratio of beams at each group. Referring to Table 5, the effective depth means the distance from the centroid of the cross-sectional dimensions of the longitudinal reinforcement in tension to the extreme compression fiber. The longitudinal reinforcement ratio is the cross-sectional area of the longitudinal reinforcement in tension divided by the effective area of the concrete cross section ($b\times d$).

The variables included in this study were the type of concrete, the type of longitudinal reinforcement and the longitudinal reinforcement ratio. The influences of these variables on the load-midspan deflection curves, bending stiffness, energy absorption and failure modes were investigated.

Beams R-S-12, P-S-12 and V-S-12 were designed as under-reinforced to obtain flexural ductile failure, i.e., the steel yielding before concrete crushing (the longitudinal reinforcement ratio ρ_s of a beam is less than the balance reinforcement ratio ρ_{sb}) (Table 5). The balance reinforcement ratio of beams reinforced with steel bars was obtained using Eq. (1) with SI units (ACI 318 2005).

$$\rho_{sb}=0.85\beta_1\frac{f'_c}{f_y}\left(\frac{600}{600+f_y}\right) \tag{1}$$

Beams R-MG-25, P-MG-25 and V-MG-25 were designed as under-reinforced to obtain GFRP rupture failure (the longitudinal reinforcement ratio ρ_f of a beam is less than the balance reinforcement ratio ρ_{fb}) (Table 5). The remaining nine concrete beams were designed as over-reinforced to obtain concrete crushing failure (the longitudinal reinforcement ratio ρ_f of a beam is higher than the balance reinforcement ratio ρ_{fb}) (Table 5). The balance reinforcement ratio of beams reinforced with either molded or pultruded GFRP grating was obtained using Eq. (2) (ACI 440 2015).

$$\rho_{fb}=0.85\beta_1\frac{f'_c}{f_{fu}}\left(\frac{E_f\varepsilon_{cu}}{E_f\varepsilon_{cu}+f_{fu}}\right) \tag{2}$$

where ρ_{sb} is the balance reinforcement ratio of the beams reinforced with steel bars, ρ_{fb} is the balance reinforcement ratio of the beams reinforced with either molded or pultruded GFRP gratings, β_1 is a compressive strength reduction factor that was obtained using Eq. (3), f'_c is the compressive strength of a concrete cylinder at 28 days (MPa), f_y is the tensile yield stress of steel bars (MPa), f_{fu} is the tensile strength of the molded and pultruded GFRP gratings (MPa), E_f is the tensile modulus of elasticity of the molded and pultruded GFRP gratings (MPa) and ε_{cu} is the ultimate compressive strain of concrete which was taken as 0.003.

$$\beta_1=\left(0.85-\left(0.05\,\frac{f'_c-28}{7}\right)\right)\qquad\geq 0.65 \tag{3}$$

2.3 Preparation of the beams, casting and test setup

The FRP rectangular cages were constructed by attaching the tension and compression reinforcement (steel bars, GFRP bars and GFRP gratings) to the SCCFRP stirrups using plastic cable ties (300 mm length). Figs. 6(a)-6(c) show the placement of the FRP rectangular cages in the formworks and the typical side view of the beams. Referring to Fig. 6(a), the FRP rectangular cages were placed inside the plywood formwork, ensuring that a clear

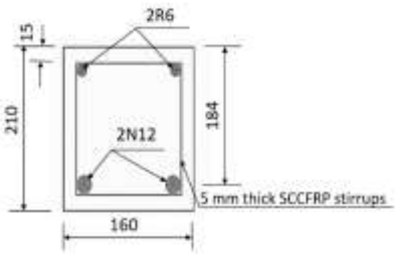

(a) Beams R-S-12, P-S-12 and V-S-12

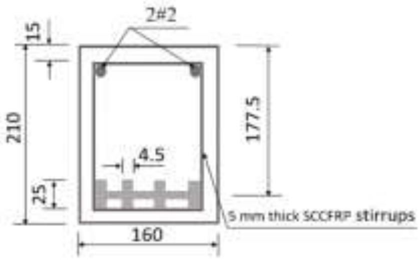

(b) Beams R-MG-25, P-MG-25 and V-MG-25

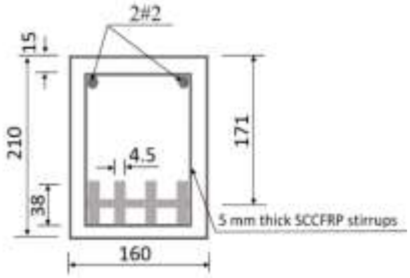

(c) Beams R-MG-38, P-MG-38 and V-MG-38

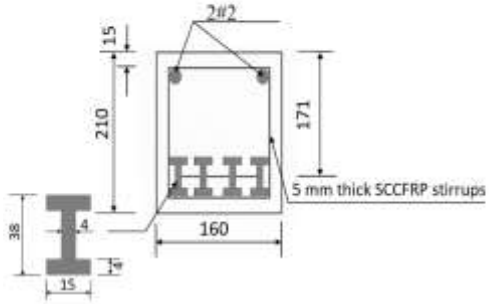

(d) Beams R-PGI-38, P-PGI-38 and V-PGI-38

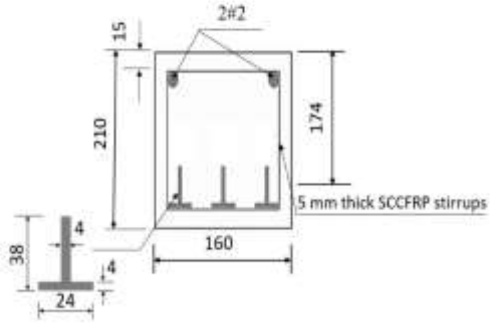

(e) Beams R-PGT-38, P-PGT-38 and V-PGT-38

Fig. 5 Details of cross-sectional dimensions of the five beams at each group (all dimensions in mm)

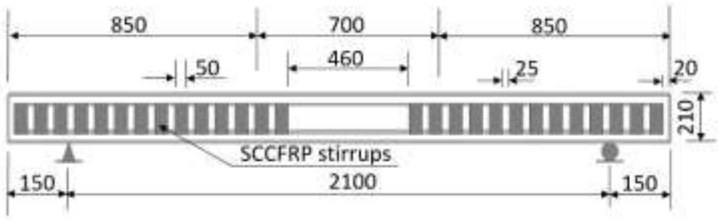

(b) Typical side view of the beams reinforced with steel bars

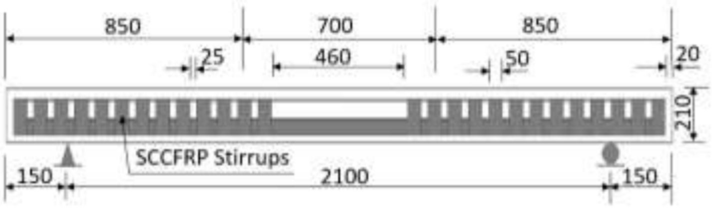

(c) Typical side view of the beams reinforced with molded or pultruded GFRP grating mesh

(a) Placement the reinforcement in the formwork,

Fig. 6 Preparation of the beam before casting (all dimensions in mm)

(a) Beams after painting

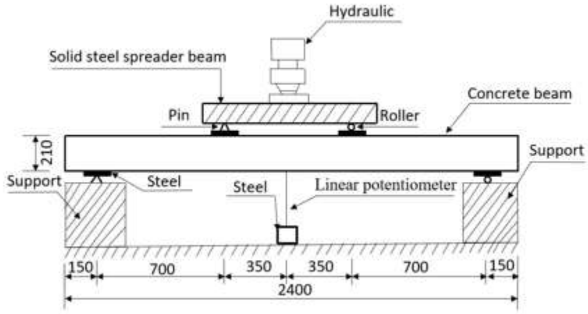

(b) Details of the test setup (all dimensions in mm)

Fig. 7 Preparation of the concrete beams and test setup

concrete cover of 15 mm was achieved. A clear spacing of 25 mm between the stirrups (SCCFRP stirrups) was achieved (Figs. 6(b) and 6(c)). In addition, no stirrups were placed within the pure bending region in the 460 mm span length, Figs. 6(b) and 6(c). The fifteen beams were cast in three batches. The reference concrete was cast in the first batch, the perlite concrete in the second batch and the vermiculite concrete in the last batch. For each batch, five concrete beams were cast and cured to the age of 28 days using wet hessian to prevent moisture loss. After 28 days curing, all beams were painted white in order to observe the crack propagation clearly during the test. Fig. 7(a) shows the beams of the reference concrete after painting.

Fig. 7(b) shows the details of the test setup. The beams were set up under simply supported condition, with a hinge at one end and a roller at the other end. The total length of a concrete beam was 2400 mm, including 2100 mm clear span length and 150 mm overhang length on each side. One linear Potentiometer (wire pot) was placed below the beams in the midspan length (Fig. 7(b)). This wire pot was used to capture the midspan deflection at two-second intervals. The load was applied using a steel spreader beam placed in the middle third of the span length within the pure bending region (Fig. 7(b)).

3. Experimental results and discussion

3.1 The load-midspan deflection curves

The load-midspan deflection curves of all beams are shown in Figs. 8-10. All the beams in all groups displayed un-cracked behavior, followed by cracked behavior. Un-cracked behavior (before concrete cracking) is the behavior of the beams from the point of origin (the point of zero load) up to the point of the first crack load (Point A), (Figs. 8-10). Cracked behavior (after concrete cracking) is the behavior of the beams from the point of first crack load (Point A) up to the point of failure (Figs 8-10). For un-cracked behavior, all beams displayed a linear behavior with exhibiting a small amount of midspan deflection (Figs. 8-10).

For cracked behavior (after the point of first crack load), Beams R-S-12, P-S-12 and V-S-12 showed elastic-perfectly plastic behavior (Figs. 8-10). Elastic-perfectly plastic behavior means that the beams displayed a linear behavior up to the point of yield load. Afterwards, a large midspan deflection was observed without exhibiting an increment in the load up to the failure (Figs. 8-10). The point of the yield load for these beams (R-S-12, P-S-12 and V-S-12) was equal to their ultimate load (Figs. 8-10). Beam R-MG-25 showed a linear behavior from the point of first crack load up to the ultimate load, without exhibiting any warning prior to failure, because Beam R-MG-25 failed by GFRP rupture which was a sudden failure (Fig. 8). Typically, for the remaining eleven beams (R-MG-38, R-PGI-38, R-PGT-38, P-MG-25, P-MG-38, P-PGI-38, P-PGT-38, V-MG-25, V-MG-38, V-PGI-38 and V-PGT-38), a linear behavior was observed from the point of first crack load up to about 80%-90% of the ultimate load. Then, the load dropped slightly due to the appearance of the cracks in compression (the top surface of a beam). Afterwards, the load was resisted leading to provide some warning prior to the concrete crushing failure (Figs. 8-10).

Table 6 shows the experimental ultimate load of the tested beams. Among the beams in the reference concrete group, Beam R-S-12 achieved an experimental ultimate load of 60kN (Table 6). The experimental ultimate load of this beam (R-S-12) was less than the experimental ultimate load of Beams R-MG-38, R-PGI-38 and R-PGT-38 by 25%, 32% and 38%, respectively (Table 6). This was because the longitudinal reinforcement ratio of Beam R-S-12 was less than the longitudinal reinforcement ratio of Beams R-MG-38, R-PGI-38 and R-PGT-38 by 72%, 80% and 72%, respectively (Table 5). Although the longitudinal reinforcement ratio of Beam R-MG-25 was higher than that of Beam R-S-12 by 56%, the corresponding experimental ultimate load of Beam R-MG-25 was almost similar to Beam R-S-12. The reason was that the tensile modulus of elasticity of the longitudinal reinforcement in Beam R-S-12 was about 92% higher than the tensile modulus of elasticity of the longitudinal reinforcement in Beam R-MG-25 (Table 3).

Table 5 Details of the beams cross-sections

Group	Beam	d (mm)*	A_s or A_f (mm^2)*	ρ_s or ρ_f*	($\rho_s/\ \rho_{sb}$*) Or ($\rho_f/\ \rho_{fb}$*)
R*	R-S-12	184.0	220	0.007	0.31
	R-MG-25	177.5	450	0.016	0.57
	R-MG-38	171.0	684	0.025	1.68
	R-PGI-38	171.0	960	0.035	2.15
	R-PGT-38	174.0	696	0.025	1.74
P*	P-S-12	184.0	220	0.007	0.33
	P-MG-25	177.5	450	0.016	0.61
	P-MG-38	171.0	684	0.025	1.78
	P-PGI-38	171.0	960	0.035	2.27
	P-PGT-38	174.0	696	0.025	1.84
V*	V-S-12	184.0	220	0.007	0.38
	V-MG-25	177.5	450	0.016	0.70
	V-MG-38	171.0	684	0.025	2.07
	V-PGI-38	171.0	960	0.035	2.64
	V-PGT-38	174.0	696	0.025	2.14

*d: Effective depth; A_s: Steel cross sectional area; A_f: Molded and pultruded GFRP grating cross sectional area; ρ_s: Steel longitudinal reinforcement ratio; ρ_f: GFRP longitudinal reinforcement ratio; ρ_{sb} Steel balance reinforcement ratio; ρ_{fb}: GFRP balance reinforcement ratio; R: Reference concrete; P: Perlite concrete; V: Vermiculite concrete

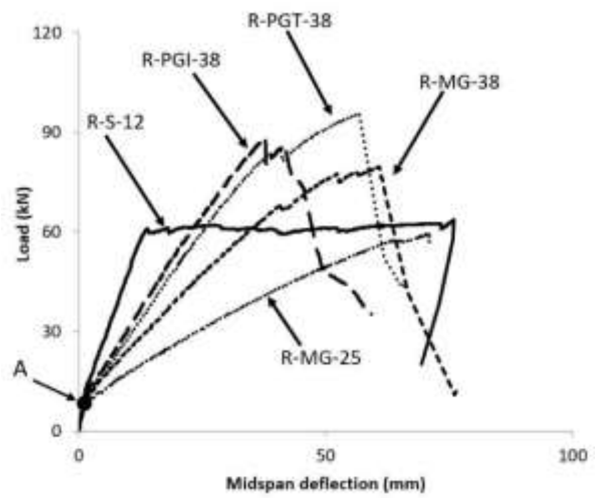

Fig. 8 Load-midspan deflection of beams in the reference concrete group

Among the beams in the perlite concrete group, Beam P-S-12 achieved an experimental ultimate load of 61 kN. The experimental ultimate load of Beam P-S-12 was less than the experimental ultimate load of Beams P-PGI-38 and P-PGT-38 by 24% and 25%, respectively (Table 6). This was because the longitudinal reinforcement ratio of Beam P-S-12 was less than the longitudinal reinforcement ratio of Beams P-PGI-38 and P-PGT-38 by 80% and 72%, respectively (Table 5). The experimental ultimate load of Beam P-MG-38 was almost similar to the experimental ultimate load of Beam P-S-12 (Table 6). Moreover, the experimental ultimate load of Beam P-MG-25 was less than the experimental ultimate load of Beam P-S-12 by 20% (Table 6). This can be attributed to the fact that the tensile modulus of elasticity of the longitudinal reinforcement in Beam P-S-12 was about 92% higher than the tensile modulus of elasticity of the longitudinal reinforcement in Beams P-MG-25 and P-MG-38 (Table 3).

Among the beams in the vermiculite concrete group, Beam V-S-12 achieved an experimental ultimate load of 61

Table 6 Test results of the tested beams at all group

Group	Beam	Experimental[a] load (kN)	Midspan deflection corresponding to the experimental load (mm)	Bending [b] stiffness (kN.m)	Analytical ultimate load (kN)	Analytical ultimate load/ experimental Load (%)
R*	R-S-12	60	13	759	63	1.05
	R-MG-25	59	70	139	42	0.71
	R-MG-38	80	60	219	68	0.85
	R-PGI-38	88	37	391	87	0.99
	R-PGT-38	96	57	277	88	0.92
P*	P-S-12	61	13	771	62	1.01
	P-MG-25	49	59	137	55	1.12
	P-MG-38	60	42	235	64	1.07
	P-PGI-38	80	32	411	82	1.03
	P-PGT-38	81	35	380	83	1.02
V*	V-S-12	61	13	771	62	1.01
	V-MG-25	57	59	159	49	0.86
	V-MG-38	64	40	263	56	0.88
	V-PGI-38	75	30	411	71	0.95
	V-PGT-38	83	45	303	72	0.87

[a]Experimental load refers to the experimental ultimate load of beams reinforced with GFRP grating or the yield load of beams reinforced with steel bars.
[b]Bending stiffness was calculated using Eq. (4) (Gere and Goodno 2011)
*R: Reference concrete; P: Perlite concrete; V: Vermiculite concrete

kN. The experimental ultimate load of Beam V-S-12 was less than the experimental ultimate load of beams V-MG-38, V-PGI-38 and V-PGT-38 by 5%, 19% and 27%, respectively (Table 6). This was because the reinforcement ratio of Beam V-S-12 was less than the reinforcement ratio of Beams V-MG-38, V-PGI-38 and V-PGT-38 by 72%, 80% and 72%, respectively (Table 5). On the other hand, the experimental ultimate load of Beam V-MG-25 was less than the experimental ultimate load of Beam V-S-12 by 7% (Table 6). This was because the tensile modulus of elasticity of the longitudinal reinforcement in Beam V-S-12 was about 92% higher than the tensile modulus of elasticity of the longitudinal reinforcement in Beam V-MG-25 (Table 3).

On a comparison of the beams in all the three groups, the experimental ultimate load of Beams R-MG-25, R-MG-38, R-PGI-38 and R-PGT-38 in the reference concrete group ranged from 3% to 25% higher than that of the corresponding beams in the perlite concrete and vermiculite concrete groups (P-MG-25, P-MG-38, P-PGI-38, P-PGT-38 V-MG-25, V-MG-38, V-PGI-38, V-PGT-38) (Table 5). This was because the compressive strength of the reference concrete at the age of testing the beams was higher than that of the perlite concrete and vermiculite concrete by 9% and 27%, respectively (Table 2). The ultimate load of the beams reinforced with steel bars (R-S-12, P-S-12 and V-S-12) ranged from 19% to 38% less than the experimental ultimate load of the beams reinforced with pultruded GFRP grating mesh (R-PGI-38, R-PGT-38, P-PGI-38, P-PGT-38, V-PGI-38 and V-PGT-38) (Table 6).

3.2 Bending stiffness and energy absorption capacity

Bending stiffness of a reinforced beam is the resistance of the beam against flexural deformation. For the beams reinforced with steel bars (R-S-12, P-S-12 and V-S-12), the bending stiffness was calculated at the point of the yield load. For the remaining beams (beams reinforced with either molded or pultruded GFRP grating mesh), the bending stiffness was calculated at the point of the ultimate load. The bending stiffness was calculated using Eq. (4) (Gere and Goodno 2011).

$$EI = \frac{Pa(3L^2-4a^2)}{48\,(\Delta_{exp})} \tag{4}$$

where EI is the bending stiffness of a reinforced beam (kN.m^2), P is the experimental load of a reinforced beam (kN) which is corresponding to the ultimate load of beams reinforced with GFRP grating or the yield load of beams reinforced with steel bars, a is the distance from the support to the nearest point load (0.7 m), L is the distance between the supports (2.1 m) and Δ_{exp} is the experimental midspan deflection corresponding to the experimental load (ultimate load or yield load) (m). The experimental load (ultimate load or yield load) and the corresponding midspan deflection of the beams in the reference concrete group, perlite concrete group and vermiculite concrete group were obtained from Figs. 8-10, respectively.

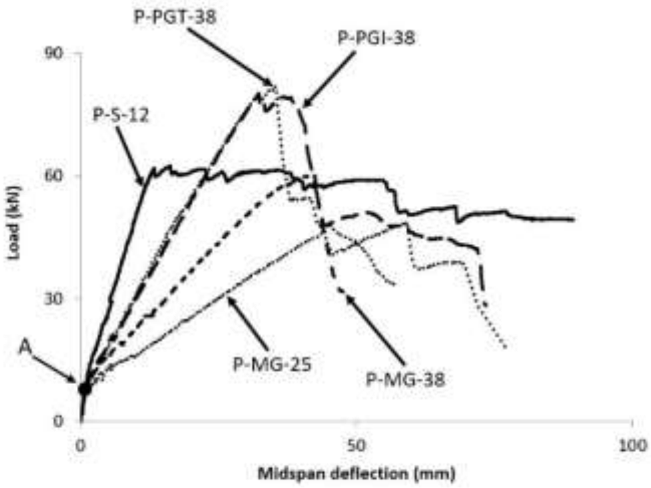

Fig. 9 Load-midspan deflection of beams in the perlite concrete group

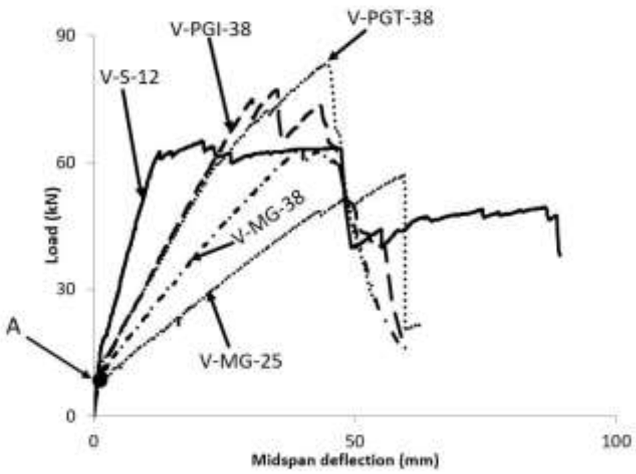

Fig. 10 Load-midspan deflection of beams in the vermiculite concrete group

The energy absorption capacities (E_1 and E_2) of all beams were calculated based on the area under the load-midspan deflection curves (Goldston *et al.* 2016). Figures. 11(a)-(b) show the method of calculating the energy absorption capacities (E_1 and E_2). For the beams reinforced with steel bars (R-S-12, P-S-12 and V-S-12), E_1 is defined as the energy absorption from the point of origin up to the point of the yield load (Fig. 11(a)), whereas E_2 is defined as the energy absorption from the point of the yield load up to the point of failure load (Fig. 11(a)). For the beams reinforced with molded or pultruded GFRP grating mesh, E_1 is defined as the energy absorption from the point of origin up to the first point of concrete crushing (Fig. 11(b)), whereas E_2 is defined as the energy absorption from the first point of the concrete crushing up to the failure (Fig. 11(b)). Beam R-MG-25 did not exhibit energy absorption capacity E_2, because it failed by GFRP rupture, which was a sudden failure.

Tables 6 and 7 show the results of the bending stiffness and the energy absorption capacities of all beams. Among the beams in the reference concrete group, the bending stiffness of Beam R-S-12 was higher than the bending stiffness of Beams R-MG-25, R-MG-38, R-PGI-38 and R-PGT-38 by 82%, 71%, 48% and 64%, respectively (Table 6). Similarly, the total energy absorption capacity (E_{total}) of Beam R-S-12 was higher than the total energy absorption capacities of Beams R-MG-25, R-MG- 38, R-PGI-38 and R-PGT-38 by 41%, 30%, 18% and 23%, respectively (Table 7). This was because the tensile modulus of elasticity of the longitudinal reinforcement in Beam R-S-12 ranged from 85% to 92% higher than the tensile modulus of elasticity of the longitudinal reinforcement in Beams R-MG-25, R-MG-38, R-PGI-38 and R-PGT-38 (Table 3). In addition, Beam R-MG-25 with $\rho_f = 1.6\%$ displayed a bending stiffness and a total energy absorption capacity of 37% and 16%, respectively, less than Beam R-MG-38 with $\rho_f = 2.5\%$ (Tables 5-7). Similarly, Beam R-PGT-38 with $\rho_f = 2.5\%$ exhibited a bending stiffness and a total energy absorption

Table 7 Results of energy absorption capacity

Group	Beam	Energy absorption E_1 (kN.mm)	Energy absorption E_2 (kN.mm)	Total energy absorption E_{total} (kN.mm)
R	R-S-12	701	3800	4501
	R-MG-25	2651	-	2651
	R-MG-38	1625	1547	3172
	R-PGI-38	1893	1807	3700
	R-PGT-38	2026	1440	3466
P	P-S-12	696	4060	4756
	P-MG-25	1216	1279	2495
	P-MG-38	2000	500	2500
	P-PGI-38	1434	2208	3642
	P-PGT-38	1431	1317	2748
V	V-S-12	467	4114	4581
	V-MG-25	1233	912	2145
	V-MG-38	1493	866	2359
	V-PGI-38	1648	1315	2963
	V-PGT-38	1478	1323	2801

* R: Reference concrete; P: Perlite concrete; V: Vermiculite concrete

capacity of 29% and 6%, respectively, less than Beam R-PGI-38 with $\rho_f = 3.5\%$ (Tables 5-7). Although the longitudinal reinforcement ratio of Beams R-MG-38 and R-PGT-38 was similar (Table 5), the corresponding bending stiffness and the total energy absorption capacity of Beam R-PGT-38 were about 21% and 8%, respectively, higher than for Beam R-MG-38 (Tables 6 and 7). This was because the tensile modulus of elasticity of the longitudinal reinforcement in Beam R-PGT-38 was about 43% higher than for Beam R-MG-38 (Table 3).

Among the beams in the perlite concrete group, the bending stiffness of Beam P-S-12 was higher than the bending stiffness of Beams P-MG-25, P-MG-38, P-PGI-38 and P-PGT-38 by 82%, 70%, 47% and 51%, respectively (Table 6). Similarly, the total energy absorption capacity of Beam P-S-12 was higher than the total energy absorption capacities of Beams P-MG-25, P-MG-38, P-PGI-38 and P-PGT-38 by 48%, 47%, 23% and 42%, respectively (Table 7). This can be attributed to the fact that the tensile modulus of elasticity of the longitudinal reinforcement in Beam P-S-12 ranged from 85% to 92% higher than the tensile modulus of elasticity of the longitudinal reinforcement in Beams P-MG-25, P-MG-38, P-PGI-38 and P-PGT-38 (Table 3). Additionally, Beam P-MG-25 with $\rho_f = 1.6\%$ displayed a bending stiffness of 42% less than for Beam P-MG-38 with $\rho_f = 2.5\%$, while manifesting almost similar total energy absorption capacity (Tables 5-7). Similarly, Beam P-PGT-38 with $\rho_f = 2.5\%$ exhibited a bending stiffness and a total energy absorption capacity of 8% and 25%, respectively, less than for Beam P-PGI-38 with $\rho_f = 3.5\%$ (Tables 5-7). Although the longitudinal reinforcement ratio of Beams P-MG-38 and P-PGT-38 was similar (Table 5), the corresponding bending stiffness and the total energy absorption capacity of Beam P-PGT-38 were about 38% and 9%, respectively, higher than of Beam P-MG-38 (Tables 6 and 7). This was because the tensile modulus of elasticity of the longitudinal reinforcement in Beam P-PGT-38 was about 43% higher than in Beam P-MG-38 (Table 3).

Among the beams in the vermiculite concrete group, the bending stiffness of Beam V-S-12 was higher than the bending stiffness of Beams V-MG-25, V-MG-38, V-PGI-38 and V-PGT-38 by 79%, 66%, 47% and 61%, respectively (Table 6). Similarly, the total energy absorption capacity (E_{total}) of Beam V-S-12 was higher than the total energy absorption capacities of Beams V-MG-25, V-MG-38, V-PGI-38 and V-PGT-38 by 53%, 49%, 35% and 39%, respectively (Table 7). This can be attributed to the fact that the tensile modulus of elasticity of the longitudinal reinforcement in Beam V-S-12 ranged from 85% to 92% higher than the tensile modulus of elasticity of the longitudinal reinforcement in Beams V-MG-25, V-MG-38, V-PGI-38 and V-PGT-38 (Table 3). Additionally, Beam V-MG-25 with $\rho_f = 1.6\%$ displayed a bending stiffness and a total energy absorption of 40% and 9%, respectively, less than Beam V-MG-38 with $\rho_f = 2.5\%$ (Tables 5-7). Similarly, Beam V-PGT-38 with $\rho_f = 2.5\%$ exhibited a bending stiffness and a total energy absorption of 26% and 5%, respectively, less than Beam V-PGI-38 with $\rho_f = 3.5\%$ (Tables 5-7). Although the longitudinal reinforcement ratio of Beams V-MG-38 and V-PGT-38 was similar (Table 5), the corresponding bending stiffness and total energy absorption capacity of Beam V-PGT-38 were about 13% and 16% higher than Beam V-MG-38 (Tables 6-7). This was because the tensile modulus of elasticity of the longitudinal reinforcement in Beam V-PGT-38 was about

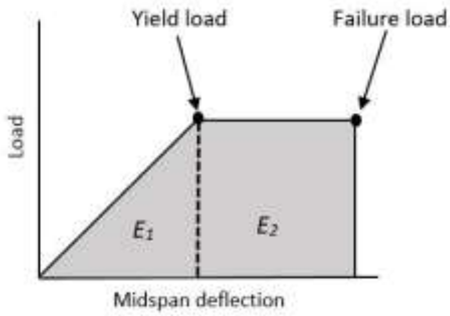

(a) Beams R-S-12, P-S-12 and V-S-12

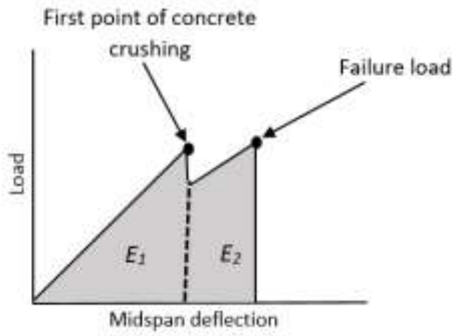

(b) Beams reinforced with molded or pultruded GFRP grating mesh

Fig. 11 Typical figures for the energy absorption capacity

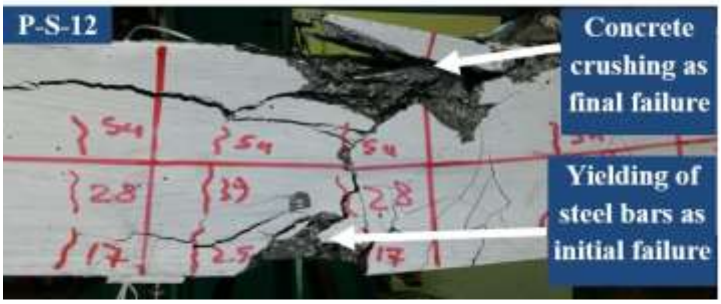

(a) Typical failure mode of Beams R-S-12, P-S-12 and V-S-12

(b) Failure mode of Beam R-MG-25

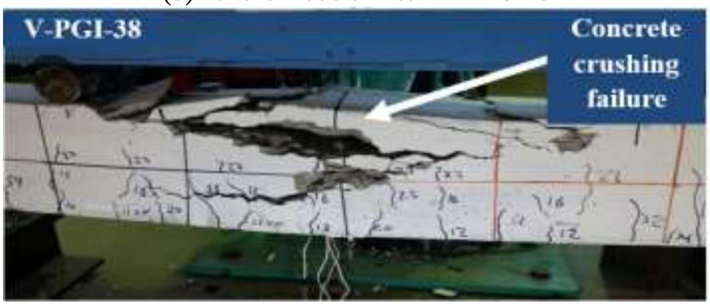

(c) Typical failure mode for the remaining eleven beams

Fig. 12 Failure modes of all the reinforced beams

43% higher than the longitudinal reinforcement in Beam V-MG-38 (Table 3).

On a comparison of the beams in all the groups, the bending stiffness of Beams R-MG-25, R-MG-38, R-PGI-38 and R-PGT-38 in the reference concrete group was slightly less than of those corresponding beams in the perlite concrete and vermiculite concrete groups (Table 6). It can be concluded that the longitudinal reinforcement ratio and the tensile modulus of elasticity of the longitudinal reinforcement influenced the bending stiffness of the beams more than the type of concrete. On the other hand, the total energy absorption capacity E_{total} of Beams R-MG-25, R-

Table 8 Experimental and design mode of failure for all beams

Group	Beam	Design mode of failure[a]	Experimental mode of failure
R*	R-S-12	Flexural tensile failure	Flexural tensile failure
	R-MG-25	GFRP rupture	GFRP rupture
	R-MG-38	Concrete crushing	Concrete crushing
	R-PGI-38	Concrete crushing	Concrete crushing
	R-PGT-38	Concrete crushing	Concrete crushing
P*	P-S-12	Flexural tensile failure	Flexural tensile failure
	P-MG-25	GFRP rupture	Concrete crushing
	P-MG-38	Concrete crushing	Concrete crushing
	P-PGI-38	Concrete crushing	Concrete crushing
	P-PGT-38	Concrete crushing	Concrete crushing
V*	V-S-12	Flexural tensile failure	Flexural tensile failure
	V-MG-25	GFRP rupture	Concrete crushing
	V-MG-38	Concrete crushing	Concrete crushing
	V-PGI-38	Concrete crushing	Concrete crushing
	V-PGT-38	Concrete crushing	Concrete crushing

[a]ACI 318 (2005) was used to design the mode of failure of beams reinforced with steel bars; ACI440 (2015) was used to design the mode of failure of beams reinforced with GFRP grating;
*R: Reference concrete; P: Perlite concrete; V: Vermiculite concrete.

MG-38, R-PGI-38 and R-PGT-38 in the reference concrete group ranged from 2% to 26% higher than of those corresponding beams in the perlite concrete group and vermiculite concrete group (Table 7). This can be because the compressive strength of the reference concrete at the age of testing the concrete beams was higher than that of the perlite concrete and vermiculite concrete by 9% and 27%, respectively (Table 2).

3.3 Mode of failure

The failure modes of all beams are shown in Figs. 12(a)-(c) and Table 8. In general, Beams R-S-12, P-S-12 and V-S-12 displayed flexural ductile failure within the pure bending region (Fig. 12(a)). The mechanism of this failure started with yielding of steel bars. Then, vertical cracks propagated upward to the compression region leading eventually to concrete crushing failure.

Concrete crushing failure was observed for all the beams reinforced with either molded GFRP grating mesh or pultruded GFRP grating mesh, except Beam R-MG-25. Beam R-MG-25 failed by GFRP rupture (Fig. 12(b)). The mechanism of failure of Beam R-MG-25 started with hairline cracks that appeared in the tensile pure bending region when the load was about 16% of the ultimate load. These cracks propagated vertically upward to the compression region and stopped at between 35 mm and 40 mm from the extreme compression fiber. Afterwards, these cracks widened gradually with increase in the load, which resulted in the GFRP rupture failure (Fig. 12(b)).

For the remaining beams (R-MG-38, R-PGI-38, R-PGT-38, P-MG-25, P-MG-38, P-PGI-38, P-PGT-38, V-MG-25, V-MG-38, V-PGI-38 and V-PGT-38), hairline cracks appeared in the tensile pure bending region when the load was about 20% of the ultimate load. These cracks propagated vertically towards the compression region and stopped at between 35 mm and 40 mm from the extreme compression fiber. Then, when the load reached between 85% and 90% of the ultimate load, two cracks appeared on the top surface at the two points of application of the load into the compression region. This eventually led to concrete crushing failure (Fig. 12(c). It can be clearly seen that the failure of all beams occurred within the pure bending region. This means that the innovative stirrups showed a significant resistance to shear failure.

On a comparison of the design failure mode and the experimental failure mode, only two beams (P-MG-25 and V-MG-25) out of the total of fifteen beams showed that the design failure mode was different from the experimental failure mode (Table 8). More experimental research studies are needed on perlite concrete and vermiculite concrete beams to determine the reasons for these differences.

3.4 Analytical ultimate load

The analytical ultimate load of the beams reinforced with either molded GFRP graing or pultruded GFRP gratings was estimated using the ACI 440 (2015) design guidelines. In addition, the analytical ultimate load of the beams reinforced with steel bars was estimated using the AS 3600 (2009). Eq. (5) has been used to calculate the analytical ultimate load for all beams (Gere and Goodno 2011).

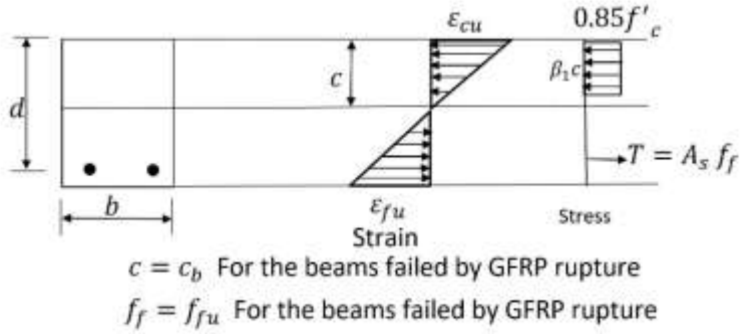

(a) Beams reinforced with molded or pultruded GFRP grating mesh

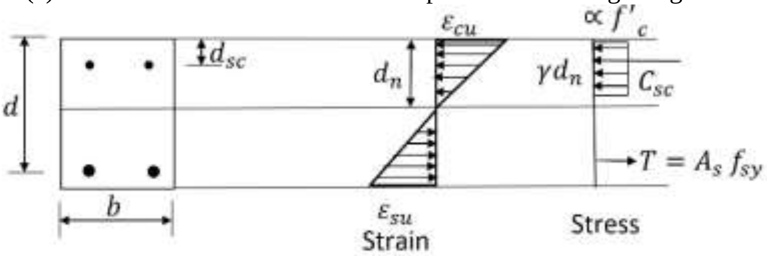

(b) Beams reinforced with steel bars

Fig. 13 Equilibrium of forces and strain compatibility of all beams

$$P = \frac{6M_n}{L} \tag{5}$$

where M_n is either the nominal moment capacity of beams reinforced with GFRP grating (M_{nf}), or the nominal moment capacity of beams reinforced with steel bars (M_{ns}), and L is the span length (2100 mm). The nominal moment capacity (M_{nf}) of the beams reinforced with either molded or pultruded GFRP grating mesh (N.mm) was calculated using Eq. (6). The ACI 440 (2015) derived this equation for beams that failed due to concrete crushing.

$$M_{nf} = \rho_f f_f \,(1 - 0.59\rho_f f_f / f'_c)\, b\, d^2 \tag{6}$$

where ρ_f is the longitudinal reinforcement ratio of a beam reinforced with GFRP grating, $\left(\rho_f = \frac{A_f}{b\,d}\right)$, A_f is the cross-sectional area of the longitudinal reinforcement in tension (mm^2), d is the distance from the centroid of the cross section of the longitudinal reinforcement in tension to the extreme compression fiber (mm), b is the width of the cross section of a reinforced concrete beam (mm), f'_c is the concrete compressive strength at the age of testing beams (MPa) and f_f is the tensile stress in the longitudinal reinforcement in tension (MPa). The f_f was obtained using Eq. (7) (MPa). This equation was derived based on the equilibrium of forces and strain compatibility in Fig. 13(a). Based on the equilibrium requirements, the compression force $C = 0.85 f'_c \beta_1 c\, b$ should be equal to the tension force $T = A_f f_f$. Thus, Eq. (7) was derived as follows

$$f_f = \sqrt{(E_f \varepsilon_{cu})^2/4 + (0.85\,\beta_1 f'_c/\rho_f) E_f\, \varepsilon_{cu}} - 0.5 E_f \varepsilon_{cu} \tag{7}$$

where E_f is the tensile modulus of elasticity of molded or pultruded GFRP grating mesh (MPa), ε_{cu} is the ultimate compressive strain of concrete which was taken as 0.003, β_1 is the reduction factor of concrete compressive strength, which was calculated using Eq. (3).

For Beam R-MG-25 that failed by GFRP rupture, Eq. (8) has been used to determine the nominal moment capacity (M_{nf}).

$$M_{nf} = A_f f_{fu}\,(d - \beta_1\, c_b/2) \tag{8}$$

where f_{fu} is the tensile strength of the longitudinal reinforcement (MPa) and c_b was obtained from the strain compatibility in Fig. 13(a) as follows

$$c_b = \left(\frac{\varepsilon_{cu}}{\varepsilon_{cu} + \varepsilon_{fu}}\right) \times d \tag{9}$$

where ε_{fu} is the tensile rupture strain of the longitudinal reinforcement, which can be obtained from Table 3. In this study, the contribution of the 6.35 mm diameter GFRP bars in the compression side of the concrete cross section was neglected for the following reasons:

1. The tensile modulus of elasticity of the 6.35 mm diameter GFRP bars is small compared to that of the steel bars.
2. The cross-sectional area of the 6.35 mm diameter GFRP bar used in compression was small (about 32 mm^2).
3. The main reason for placing the 6.35 mm diameter GFRP bars in compression was to control the spacing between stirrups.
4. The ACI 440 (2015) recommended neglecting the contribution of the GFRP bars to load resistance in a compression member.

For beams reinforced with steel bars (R-S-12, P-S-12 and V-S-12), the AS 3600 (2009) derived Eq. (10) to determine the nominal moment capacity for under-reinforced beams.

$$M_{ns} = A_s\, f_{sy} \left(d - {}^{\gamma\, d_n}\!/_2 \right) \tag{10}$$

where A_s is the cross-sectional area of the steel bars in tension (mm^2), f_{sy} is the yield tensile stress of the steel bars (MPa), d is the distance from the centroid of the steel bars in tension to the extreme compression fibre (mm). Based on the equilibrium requirements (Fig. 13(b)), the compression forces $C = \propto f'_c\, \gamma d_n\, b$ and $C_{cs} = E_s\, A_{sc}\, \varepsilon_{sc}$ should be equal to the tension force $T = A_s\, f_{sy}$. Thus, the distance from the neutral axis to the extreme compression fiber, d_n (mm) can be calculated as follows

$$m\, {d_n}^2 + n\, d_n - x = 0 \tag{11}$$

where

$m = \propto\ f'_c\, \gamma\, b$

$n = \left(E_{sc}\, A_{sc}\, \varepsilon_{cu} - A_s\, f_{sy} \right)$

$x = (E_{sc}\, A_{sc}\, \varepsilon_{cu}\, d_{sc})$

$\propto = 1 - 0.003\, f'_c$ $\quad 0.67 \leq \propto \leq 0.85$

$\gamma = 1.05 - 0.007\, f'_c$ $\quad 0.67 \leq \gamma \leq 0.85$

where m, n and x are the material parameters depending on the material properties, f'_c is the concrete compressive strength at the age of testing the beams (MPa), b is the width of the beams cross section (mm), E_{sc} is the tensile modulus of elasticity of the steel bars in compression (MPa) as obtained from Table 3, A_{sc} is the cross sectional area of the steel bars in compression (mm^2), ε_{cu} is the compressive ultimate strain of concrete, taken as 0.003, and d_{sc} is the distance from the centroid of the steel bars in compression to the extreme compression fiber (mm) (Fig. 13(b)).

It can be clearly seen that there was good agreeme nt between the analytical and the experimental ultimate load for all beams, except Beam R-MG-25 (Table 6). Beam R-MG-25 showed an experimental ultimate load of 29% higher than the analytical ultimate load (Table 6).

4. Conclusions

This paper investigated the flexural behavior of concrete beams reinforced with either steel bars, molded GFRP grating mesh or pultruded GFRP grating mesh, under four point-bending. The influences of the type of concrete, the type of longitudinal reinforcement and the longitudinal reinforcement ratio on the load-midspan deflection curves, bending stiffness, energy absorption and failure modes were investigated. Based on the test results, the following conclusions can be obtained:

- The ultimate load of the beams reinforced with pultruded GFRP grating mesh ranged from 19% to 38% higher than the ultimate load of the beams reinforced with steel bars.
- Increasing the longitudinal reinforcement ratio of the beams reinforced with molded or pultruded GFRP grating mesh from 0.016 to 0.035 led to an increase in the bending stiffness to about 67%.
- The bending stiffness of a reinforced concrete beam was slightly influenced by the type of concrete. However, the bending stiffness of a reinforced concrete beam was significantly influenced by the longitudinal reinforcement ratio and the tensile modulus of elasticity of the longitudinal reinforcement.
- The type of concrete influenced the ultimate load and the energy absorption of the beams more than the bending stiffness.
- The energy absorption capacity E_1 of the beams reinforced with molded or pultruded GFRP grating mesh was significantly higher than of those beams reinforced with steel bars.
- The total energy absorption capacity (E_{total}) of beams reinforced with steel bars was higher than of those beams reinforced with either molded GFRP grating mesh or pultruded GFRP grating mesh.
- Fourteen beams out of a total of fifteen showed good agreement between the experimental and analytical ultimate load.
- For all beams, failure occurred within the pure bending region, which means that the innovative SCCFRP stirrups showed significant resistance to shear failure.
- The use of perlite concrete or vermiculite concrete in combination with molded GFRP grating mesh or pultruded GFRP grating mesh as longitudinal reinforcement not only reduces the weight of a structure, but also can eliminate the chloride-induced corrosion problem

Acknowledgments

The authors would like to express their gratitude to the Scavenger Company, Australia for supplying the molded and pultruded GFRP grating mesh for this study. The authors would also like to acknowledge the V-rod company for supplying the GFRP bars and to thank the Ausperl, Sydney, Australia for providing the expanded perlite and vermiculite for this study. The authors are indebted to the Technical Officers at the University of Wollongong, Australia for their ongoing advice during the experimental program. Last but not the least, the second author would like to thank the Higher Committee for Education Development in Iraq for their financial support.

References

Abdeen, M.A.M. and Hodhod, H. (2010), "Experimental investigation and development of artificial neural network model for the properties of locally produced lightweight aggregate concrete", *Engineering*, **2**(6), 408-419.

ACI Committee 318 (2005), "Building Code Requirements for Structural Concrete and Commentary American Concrete Institute", Detroit, USA.

ACI Committee 440 (2015), “Guide for the design and construction of structural concrete reinforced with FRP Bars”, American Concrete Institute, Farmington Hills (MI), USA.

Alhussainy, F., Hasan, H.A., Sheikh, M.N. and Hadi, M.N.S. (2017), “A new method for direct tensile testing of concrete”, *J. Test. Eval.*, https://doi.org/10.1520/JTE20170067.

Alsayed, S.H. (1998), “Flexural behavior of concrete beams reinforced with GFRP bars”, *Cement Concrete Compos*., **20**(1), l-11.

American grating (2015), “Manufacture of Fiberglass Grating Structural”, & 1191 Centre Point Drive Henderson, NV 89074, USA. https://www.americangrating.com/, accessed 3 March 2016.

AS 1012 (1999), “Methods of testing concrete”, Standards Australia Limited; NSW, Australia.

AS 1391-2007 (2007), “Metallic Materials-Tensile Testing at Ambient Temperature”, Standards Australia Limited; NSW, Australia.

AS 2758.1(2009), “Concrete aggregates”, Standards Australia Limited; NSW, Australia.

AS 3600 (2009), “Concrete structures”, Standards Australia Limited; NSW, Australia.

ASTM D3039 (2000), “Standard test method for tensile properties of polymer matrix composite materials”.

ASTM D7205 (2011), “Standard Test Method for Tensile Properties of fiber Reinforced Polymer Matrix Composite Bars”, American Society for Testing and Materials, West Conshohocken, PA, USA.

Ausperl (2012), “*Australia Home Page*”, Available from: http://www.ausperl.com/, accessed 13 may 2015.

Barris, C., Torres, L., Turon, A., Baena, M. and Catalan, A. (2009), “An experimental study of the flexural behavior of GFRP RC beams and comparison with prediction models”, *Compos. Struct.*, **91**(3), 286-295. https://doi.org/10.1016/j.compstruct.2009.05.005.

Biddah, A. (2006), “Structural reinforcement of bridge decks using pultruded GFRP grating”, *Compos. Struct.*, **74**(1), 80-88. https://doi.org/10.1016/j.compstruct.2005.03.016.

Chen, B.L. and Wang, L.G. (2015), “Experimental study on flexural behavior of splicing concrete-filled GFRP tubular composite members connected with steel bars”, *Steel Compos. Struct.*, **18**(5), 1129-1144. http://dx.doi.org/10.12989/scs.2015.18.5.1129.

Demirboga, R., Orung, I. and Gul, R. (2001), “Effects of expanded perlite aggregate and mineral admixtures on the compressive strength of low-density concretes”, *Cement Concrete Res.*, **31**(11), 1627-1632. https://doi.org/10.1016/S0008-8846(01)00615-9.

El-Nemr, A., Ahmed, E.A. and Benmokrane, B. (2013), “Flexural behavior and serviceability of normal- and high-strength concrete beams reinforced with glass fiber-reinforced polymer bars”, *ACI Struct. J.*, **110**(6), 1077.

Gere, J.M. and Goodno, B.J. (2011), “Mechanics of Materials”, *Cengage Learning*.

Goldston, M.W., Remennikov, A. and Sheikh, M.N. (2016), “Experimental investigation of the behavior of concrete beams reinforced with GFRP bars under static and impact loading”, *Engineering Structures,* **113**, 220-232.

Hanson Construction and Building Materials (2017), “Australia Pty Ltd”, http://www.hanson.com.au, accessed 3 April 2017.

Kalpana, V.G. and Subramanian, K. (2011), “Behaviour of concrete beams reinforced with GFRP BARS”, *J. Reinforced Plastics Compos*., **30**(23), 1915-1922.

Larralde, J. (1992), “Feasibility of FRP molded grating-concrete composites for one-way slab systems”, (Ed., White, T.D.), *Proceedings of the ASCE 1992 Materials Engineering Congress*, New York, USA, ASCE, 645-54.

Oktay, H., Yumrutas, R. and Akpolat, A. (2015), “Mechanical and thermo-physical properties of lightweight aggregate concretes”, *Constr. Build. Mater.*, **96**, 217-225. https://doi.org/10.1016/j.conbuildmat.2015.08.015.

Rashad, A.M. (2016a), “A synopsis about perlite as building material - A best practice guide for Civil Engineers”, *Constr. Build. Mater.*, **121**, 338-353. https://doi.org/10.1016/j.conbuildmat.2016.06.001.

Rashad, A.M. (2016b), “Vermiculite as construction material - A short guide for Civil Engineers”, *Constr. Build. Mater.*, **125**, 53-62. https://doi.org/10.1016/j.conbuildmat.2016.08.019.

Scavenger (2015), “Molded and pultruded glass-fiber grating mesh”, & 15 Waverley Drive, Unanderra, NSW 2526, Australia. https://scavengersupplies.com.au, accessed 29 September 2015.

Schackow, C., Effting, M.V., Folgueras, S., Güths, G.A. and Mendes, G.A. (2014), “Mechanical and thermal properties of lightweight concrete with vermiculite and EPS using air-entraining agent”, *Constr. Build. Mater.*, **57,** 190-197. https://doi.org/10.1016/j.conbuildmat.2014.02.009.

Sika (2012), “*Sika Australia Home Page*”, Available from: http://aus. sika.com/en/solutions products/document library/product data sheets/product-datasheets-sika-p.html, accessed 5 January 2017.

V-Rod (2012), “Composite Reinforcing Rods Technical Data Sheet”, Large Bay SA, Australia, accessed 3 February 2017.

Xiao, Y., Zeng, L., Cui, Z., Jin, S. and Chen, Y. (2017), “Experimental and analytical performance evaluation of steel beam to concrete-encased composite column with unsymmetrical steel section joints”, *Steel Compos. Struct.*, **23**(1), 17-29. https://doi.org/10.12989/scs.2017.23.1.017.

Xiong, W., Cai, C.S., Xiao, R. and Zhang, Y. (2012), “Design strategy of hybrid stay cable system using CFRP and steel materials”, *Steel Compos. Struct.*, **13**(1), 47-70. http://dx.doi.org/10.12989/scs.2012.13.1.047.

BU